Synthesis of pitch-derived carbon anodes for high-performance potassium-ion batteries

JIANG Ming-chi, SUN Ning*, YU Jia-xu, WANG Ti-zheng,
Razium Ali Somoro, JIA Meng-qiu*, XU Bin*

（*State Key Laboratory of Organic-Inorganic Composites*, *Beijing Key Laboratory of Electrochemical Process and Technology for Materials*, *Beijing University of Chemical Technology*, *Beijing* 100029, *China*）

Abstract: Potassium-ion batteries (PIBs) hold promise for large-scale energy storage, necessitating the development of high-performance anode materials. Carbons with the advantage of structural versatility, are recognized as the most promising anode materials for their commercialization, however the relationship between the carbon anode structure and its electrochemical performance remains unclear. A series of pitch-based soft carbons with different structures were fabricated using carbonization temperatures in the range 600–1400 °C, and their changes in carbon configuration and K-storage performance as a function of carbonization temperature were investigated. Correlations between the carbon crystal size and the low-potential plateau region capacity and between the degree of structural disorder of the carbons with their sloping region capacity were revealed. Among all samples, that obtained by carbonization at 700 °C had a relatively high degree of disorder and a large interlayer spacing, and had a high reversible capacity of 329.4 mAh g^{-1} with a high initial coulombic efficiency of 72.81%, and maintained a high capacity of 144.2 mAh g^{-1} at the current rate of 5 C. These findings improve our fundamental understanding of the K-storage process in carbon anodes, and thus facilitate the advance of PIBs.

Key words: Potassium-ion batteries; Pitch; Carbon material; Anode; Mechanism

1 Introduction

Lithium-ion batteries (LIBs) have been widely developed on a large scale of modern society, such as portable electronic devices and electric vehicles (EVs). However, the continuous consumption and the low content of lithium resources lead to the much-increased price of LIBs, which greatly restrict the further development of LIBs[1,2]. Due to its resource abundance, low cost and relatively low redox potential of K^+/K (−2.93 V vs. standard hydrogen electrode), potassium-ion batteries (PIBs) have been considered as a promising alternative to LIBs, especially in the field of large-scale energy storage[3,4]. Graphite, which is commonly used as the anode material in LIBs, can also be utilized to store potassium (K) in the form of KC_8. This can provide a theoretical K-storage capacity of 279 mAh g^{-1} with a low-potential plateau region[5,6]. However, because of the large ionic size of K^+ (1.38 Å vs. 0.76 Å for Li^+), a huge volume change of about 60% will occur during the storage of K^+ in graphite with a small interlayer spacing (0.337 nm)[7,8]. Besides, the sluggish K^+ kinetics leads to inadequate cycle stability and rate performance, which restricts the further development of PIBs[8,9].

Amorphous carbon materials have gained significant interest as low-cost, eco-friendly anode materials for PIBs due to their wide availability[10,11]. These materials can be classified as either hard carbons or soft carbons, depending on their structure and electrochemical performance. Hard carbons have a highly disordered carbon structure, abundant defect sites, and the much larger interlayer spacing than graphite, which is beneficial to K^+ transportation in the carbon structure[12-15]. As a result, hard carbon anodes could deliver superior rate performance than graphite an-

Received date: 2024-04-26; **Revised date:** 2024-06-11
Corresponding author: SUN Ning, Associate Professor. E-mail: ningsun@mail.buct.edu.cn;
JIA Meng-qiu, Professor. E-mail: jiamq@mail.buct.edu.cn;
XU Bin, Professor. xubin@mail.buct.edu.cn.

Author introduction: JIANG Ming-chi, Ph.D candidate. E-mail: 1149937501@qq.com

odes[16,17]. Nevertheless, the lack of regularly arranged carbon layers in hard carbons also results in a typical K-storage curve in a high-potential sloping region, which is unsuitable for practical application as anode materials[18-20]. Soft carbons exhibit a higher disordered degree and larger interlayer spacing compared to graphite, while also possessing a higher level of graphitization and more regularly arranged carbon layers than hard carbons. Thus, it has been recognized as a promising candidate for anode materials in PIBs[21-23]. The charge-discharge curves of soft carbons consist of a sloping region in high potential and a plateau region in low potential, leading to enhanced K-storage capacity and rate performance, enabling a higher output voltage of assembled full-cells[24,25].

Pitch is a low-cost industrial by-product that has high carbon content and abundant resources, and the pitch-based carbons are typically soft carbon in nature with a disordered structure, and good electrical conductivity[26,27]. Constructing porous structure has been proved to be an efficient strategy to facilitate K ion storage in pitch-derived soft carbons. Liu et al.[23] fabricated a mesoporous carbon (MCUF) using mesophase pitch as a carbon precursor and nano-$CaCO_3$ as a hard template. The derived MCUF with a well-developed mesoporous structure and ultrathin framework delivered a much higher K-storage capacity of 343 mAh g^{-1} than the pitch-based soft carbons (258 mAh g^{-1}). Additionally, surface modification is also a commonly used method to enhance the K-storage performance of carbon anodes. Ma et al.[27] reported a nitrogen and phosphorus dual-doped coal tar pitch based porous carbon (NPPC). The obtained NPPC with a large interlayer spacing of 0.421 nm and high contents of N (3.68%, atomic percent) and P (3.15%) element exhibited an initial reversible capacity of 301 mAh g^{-1} at a current density of 25 mA g^{-1}, with a retained capacity of 133 mAh g^{-1} at 5 A g^{-1}. The porous structure and heteroatom functional groups typically contribute to the surface adsorption mechanism for K^+ storage, which has been well clarified in previous literatures. Nevertheless, the correlation between the K-storage property and microcrystalline structure still remains unclear, which requires a systematical investigation to comprehensively understand their evolution with pyrolysis temperature.

In this work, a series of pitch-based soft carbon materials with different microstructures have been synthesized by varying the carbonization temperature, and their electrochemical performances are explored to determine the optimal carbon for PIB anode. Among all, MTP700 delivered a high reversible K-storage capacity of 329.4 mAh g^{-1}, corresponding to a high initial coulombic efficiency (ICE) of 72.81%. Due to its relatively higher disordered degree and larger interlayer spacing, a high capacity of 144.2 mAh g^{-1} was achieved at a high current rate of 5 C, indicating its excellent electrochemical K-storage performance.

2 Experimental

2.1 Synthesis method

The raw pitch material is a national standard medium temperature pitch purchased from Handan Jinghao Chemical Co., Ltd. (Product batch number: No. JH-3). The pitch blocks were crushed into powder and spread evenly in an alumina boat, which was then placed in the central zone of a tube furnace. The temperature was ramped up to 600, 700, 800, 1 000, 1 200 and 1 400 °C at a rate of 5 °C min^{-1}, and carbonized for 2 h under an argon atmosphere. After cooling to room temperature, the samples were washed with diluted hydrochloric acid and deionized water to remove the soluble ash and impurities. The pitch-based carbons prepared at different carbonization temperatures were designated as MTPX, where X represents the pyrolysis temperature.

2.2 Characterization

The structural characteristics of the synthesized pitch-based carbons were analyzed using various techniques. The thermal stability of the raw pitch material was investigated using a thermal analyzer (NETZSCH STA 449C) in a temperature range from room temperature to 1 000 °C with a rate of 5 °C min^{-1} under N_2 atmosphere. Morphological examination was carried out using a scanning electron microscope (SEM, HITACHI S4800) and a field emission trans-

mission electron microscope (TEM, FEI Tecnai G2 F30). X-ray diffraction (XRD) was conducted using a Rigaku Ultima IV instrument, while Raman spectroscopy was performed with a Renishaw in Via Reflex spectrometer.

2.3 Electrochemical measurements

The working electrode was coated on a copper foil current collector with pitch-based carbon, conductive agent (Super-P), and binder (CMC) at mass ratios of 8∶1∶1, which was vacuum-dried and then cut into disks with a diameter of 8 mm, and the mass loading of active materials was kept at about 1.0 mg cm^{-2}. The counter electrode was metallic potassium foil, and the electrolyte consisted of 0.8 mol L^{-1} KPF_6 dissolved in a 1∶1 volume ratio of ethylene carbonate (EC) and diethyl carbonate (DEC) (0.8 mol L^{-1} KPF_6 EC/DEC=1∶1 *v*/*v*), with fiberglass as the separator. The CR2025 coin-typed half-cell was assembled inside a glove box (Mikrouna-Super) under an argon atmosphere with low levels of water and oxygen content (both below 0.1×10^{-6}). The electrochemical tests were conducted in a multichannel battery test system (Neware CT-4008T).

3 Results and discussion

3.1 Morphology and microstructures

The morphology of the prepared pitch-based pyrolytic carbons was characterized using SEM as shown in Fig. 1. At the low carbonization temperature (MTP600, MTP700, MTP800), MTP samples resemble small and scattered blocks. As the carbonization temperature increases (MTP1000, MTP1200, MTP1400), the carbon blocks become larger with a distinct layered structure, which is ascribed to the increased graphitization degree of MTP samples with increasing the carbonization temperature.

The prepared MTP samples were characterized using high-resolution TEM (HRTEM) equipped with selected area electron diffraction (SAED) (Fig. 2). The representative MTP600 exhibits a highly disordered carbon configuration with an invisible carbon arrangement, with an interlayer spacing of 0.354 nm, confirming its highly disordered degree at low pyrolysis temperatures. As the carbonization temperature increases, more short-range ordered and parallel carbon layers are observed, evidenced by the intensified diffraction rings in SAED patterns. As a result, the interlayer spacing gradually decreases, in the order of 0.352 nm for MTP700, 0.351 nm for MTP800, 0.350 nm for MTP1000, and 0.347 nm for MTP1200. The MTP1400 exhibits an incompletely graphitized structure with a minimum carbon interlayer spacing of 0.346 nm, and many highly oriented carbon layers can be observed. This trend shows that as the carbonization temperature of MTP increases, the carbon structure transitions from a disordered and less ordered car-

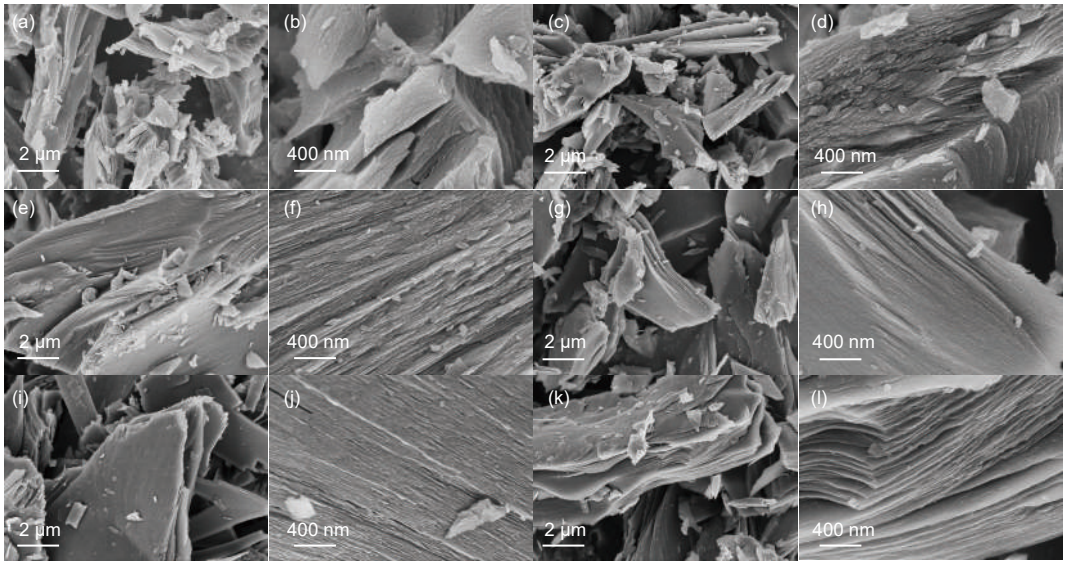

Fig. 1　SEM images of MTP samples: (a, b) MTP600, (c, d) MTP700, (e, f) MTP800, (g, h) MTP1000, (i, j) MTP1200 and (k, l) MTP1400

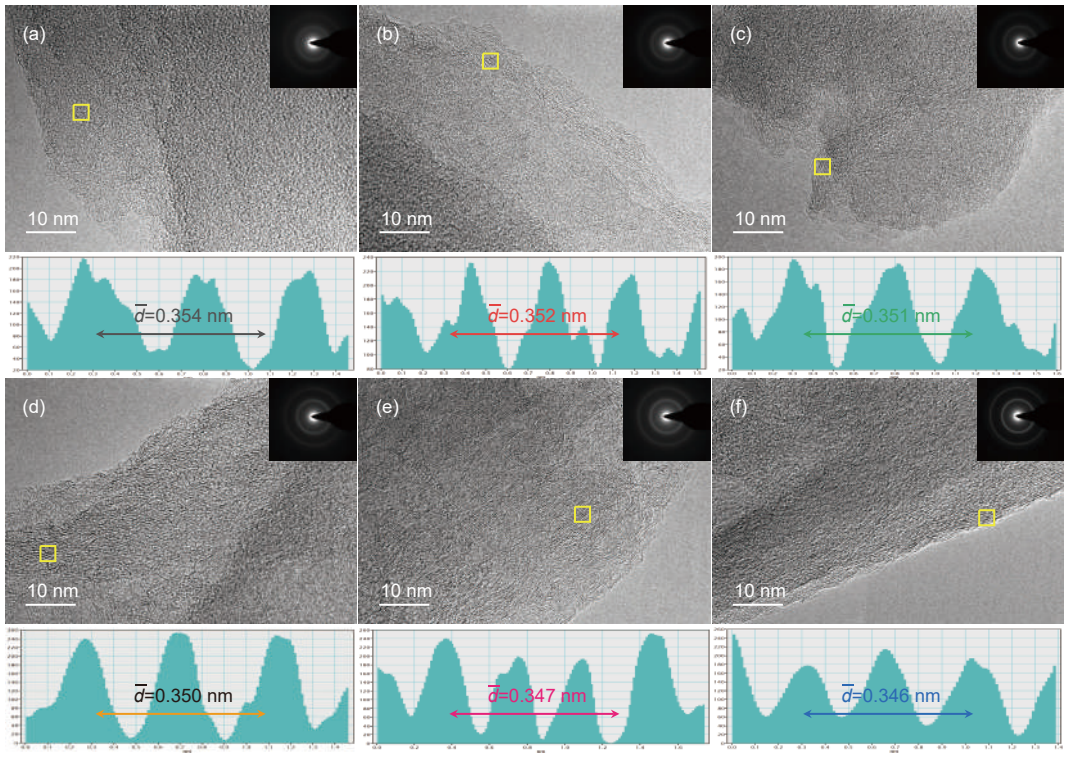

Fig. 2 HRTEM and SAED images of MTP samples: (a) MTP600, (b) MTP700, (c) MTP800, (d) MTP1000, (e) MTP1200 and (f) MTP1400

bon layer arrangement to a more regular and graphitized microcrystalline structure.

Thermogravimetric analysis (TG) and derivative thermogravimetry (DTG) were conducted to evaluate the pyrolysis characteristics of the raw pitch material. Fig. 3a shows a slight mass decrease corresponding to water desorption in the pitch raw material before 100 °C. As the temperature rises within the range of 100–600 °C, the mass decreases significantly, reaching its maximum mass loss rate at 300 °C, which corresponds to the evaporation of volatile components and small molecules in the pitch raw material. Subsequently, the rate of mass change slows noticeably above 600 °C, indicating the near completion of carbonization of pitch. The microcrystalline structures of the derived MTPs were characterized by XRD as

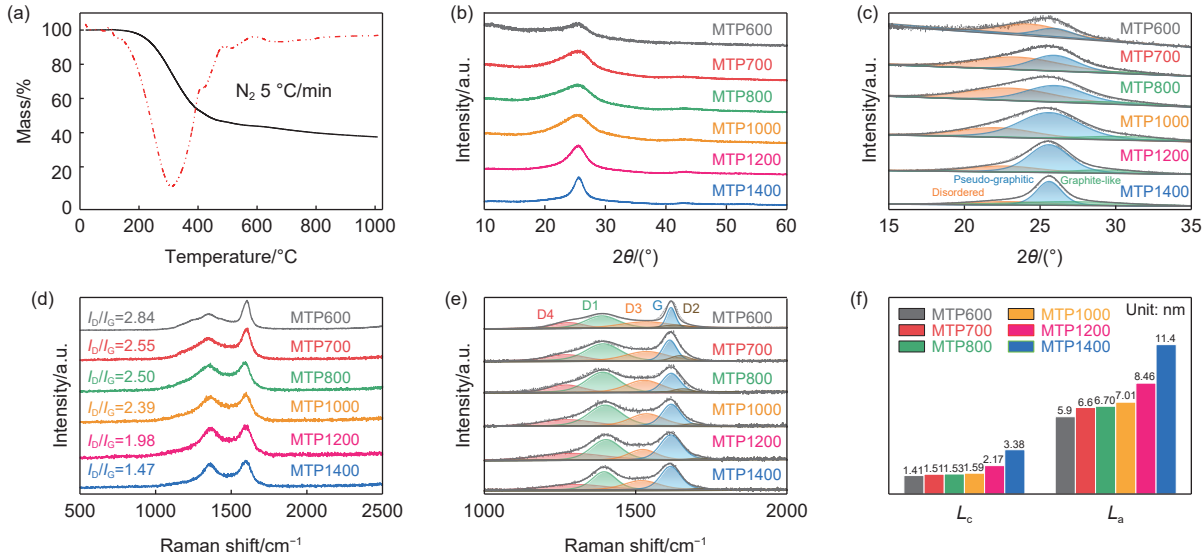

Fig. 3 (a) TG and DTG curves, (b, c) XRD patterns and fitted (002) peaks, (d, e) Raman spectroscopy and fitted curves and (f) the crystalline parameters of the MTP samples

shown in Fig. 3b. All carbon materials exhibited broad peaks around 24°, which correspond to the (002) crystal plane of the carbon, typical of the amorphous nature[28,29]. The diffraction peaks gradually become sharper and shift to higher degree with increasing the carbonization temperature, confirming the increased graphitization and structural order degree of the carbon materials. The interlayer spacing of the carbon materials could be obtained by using the Bragg equation[30,31]. The calculated interlayer spacing for MTP600 is 0.354 nm (Table 1). As the pyrolysis temperature increases, the interlayer spacing of MTPs gradually decreases from 0.351 nm for MTP800 to 0.350 nm for MTP1000 and then 0.347 nm for MTP1200, which is consistent with HRTEM. In the case of MTP1400, the noted interlayer spacing of 0.346 nm is still larger than the interlayer spacing of graphite (0.337 nm). To attain more detailed carbon structure information, the (002) peaks were further deconvoluted according to the disordered band, pseudo-graphitic band and the graphite-like band, as displayed in Fig. 3c. MTP600 is consisted of a disordered band (68.94%) and a pseudo-graphitic band (31.06%), indicating its highly disordered carbon structure. With the increase of pyrolysis temperature, a graphite-like band appears in MTP700 sample, and the ratio steadily increases from 4.69% for MTP700 to 8.17% for MTP800, and then 11.80% for MTP1000 and 12.58% for MTP1200, which eventually reach 32.11% for MTP1400, revealing the increased graphitization degree[32,33].

The Raman spectra are shown in Fig. 3d, with all MTP samples exhibiting typical *D* and *G* peaks located at ~1 350 and ~1 590 cm^{-1}, representative of defect-related structures and the graphitic structures in carbon materials, respectively. The area ratio of the *D* peak to *G* peak (I_D/I_G) was used to analyze the defect content and graphitization degree in the carbon materials. MTP600 has the highest I_D/I_G value of 2.84, which then gradually decreases with the increase of carbonization temperature: MTP700 (2.55), MTP800 (2.50), MTP1000 (2.39), MTP1200 (1.98), MTP1400 (1.47), confirming the decreased defect contents and enhanced graphitization degree of the carbon materials. The Raman *D* peaks can be divided into *D*1, *D*2, *D*3 and *D*4 (Fig. 3e), and the I_{D1}/I_G ratio could be used to assign the defects or edge sites in carbon materials. MTP600 with a highly disordered degree exhibits a I_{D1}/I_G value of 2.22, which progressively decreases to 2.00, 1.89, 1.73, 1.13 and 0.93 for MTP700, MTP800, MTP1000, MTP1200 and MTP1400, respectively, demonstrating the decreased defect content in MTP carbon materials when the carbonization temperature increases[31-33].

Furthermore, the microcrystal size vertical (L_c) to the carbon layers was calculated from the Scherrer formula $\left(L=\frac{k\lambda}{\beta\cos\theta}\right)$ based on the (002) diffraction peak. Considering the inconspicuous (100) peak, the size of carbon microcrystals in the direction parallel (L_a) to the carbon layers was obtained based on Raman results using the equation $\left(L_a(\mathrm{nm})=2.4\times10^{-10}\times\lambda^4\times\left(\frac{I_G}{I_D}\right)\right)$, where λ represents the wavelength of the Raman spectroscopy laser (514 nm) and the I_G/I_D is the area ratio of the *G* peak and the *D* peak[34-36]. As shown in Fig. 3f, MTP600 has the smallest L_a value of 5.90 nm and L_c of 1.41 nm, indicating its highly disordered microcrystalline structure and smallest grain size. As the carbonization temperature increases, the L_a value of MTP increases

Table 1　Structural properties and electrochemical performance of MTP samples

Samples	d_{002}/nm	I_D/I_G	initial charge/discharge cycle		Capacity 5 C/mAh g^{-1}
			Charge/mAh g^{-1}	ICE/%	
MTP600	0.354	2.84	285.3	64.9	99.9
MTP700	0.352	2.55	329.4	72.8	144.2
MTP800	0.351	2.50	309.2	68.0	138.1
MTP1000	0.350	2.39	262.7	66.9	118.6
MTP1200	0.347	1.98	261.6	62.8	105.5
MTP1400	0.346	1.47	253.2	60.4	92.0

from 6.57 nm (MTP700) to 11.40 nm (MTP1400), and the L_c value exhibits the same trend with an increase from 1.51 nm for MTP700 to 3.38 nm for MTP1400, confirming increased graphitization degree and microcrystalline size, which is consistent with the trends observed in HRTEM and XRD.

3.2 Electrochemical performance of MTPs

A half-cell assembled with MTP as the active material was subjected to a cyclic voltammetry (CV) test at a scan rate of 0.1 mV s^{-1} within a potential range of 0.01–3.0 V (vs. K^+/K) (Fig. 4). The CV curve of MTP600 exhibits a peak at high potential without obvious oxidation/reduction peaks at low potentials. This may be due to the incomplete carbonization of the pitch at a low temperature of 600 °C. HRTEM confirms the lack of parallel arranged carbon layers in the carbon structure and a high degree of disorder. In this case, the storage of potassium (K^+) primarily occurs through adsorption at the surface and defect sites. As the carbonization temperature increases, the CV curves of MTP700 and MTP800 show oxidation peaks around 0.5 V, which should correspond to K-storage between the carbon interlayers. Moreover, the weaker peaks in the voltage range of 0.5–2.0 V could be attributed to the adsorption K-storage process. As the carbonization temperature increases further, the oxidation peak at 0.5 V becomes sharper and stronger, and the peaks at high voltages gradually weakens. This could be attributed to the enhanced degree of graphitization, regularization of the microcrystalline structure, and reduction in defects within the carbon material when the carbonization temperature rises.

To investigate the K-storage performance of MTP samples, galvanostatic charge/discharge (GCD) tests were carried out in a K-ion half-cell at a current rate of 0.1 C (1 C = 279 mA g^{-1}) (Fig. 5). MTP600 exhibits a reversible K-storage capacity of 285.4 mAh g^{-1} with an ICE of 64.9%. Due to its highly disordered structure and relatively lower carbonization degree, the GCD curves primarily exhibit the high-potential sloping region, different from those of other carbon materials. Subsequently, the fully carbonized MTP700 structure, which contains abundant defects and adsorption K-storage sites, results in a highly reversible high-potential sloping region with the highest reversible specific capacity of 329.4 mAh g^{-1} and the highest ICE of 72.8%. As the carbonization temperature increases, the graphitization degree of the carbon material increases while the interlayer spacing and the defect sites decrease. Consequently, the potassium storage capacity in the high-potential region and the overall potassium storage potential gradually diminishes while the plateau becomes more pronounced. The observed trend agrees well with the

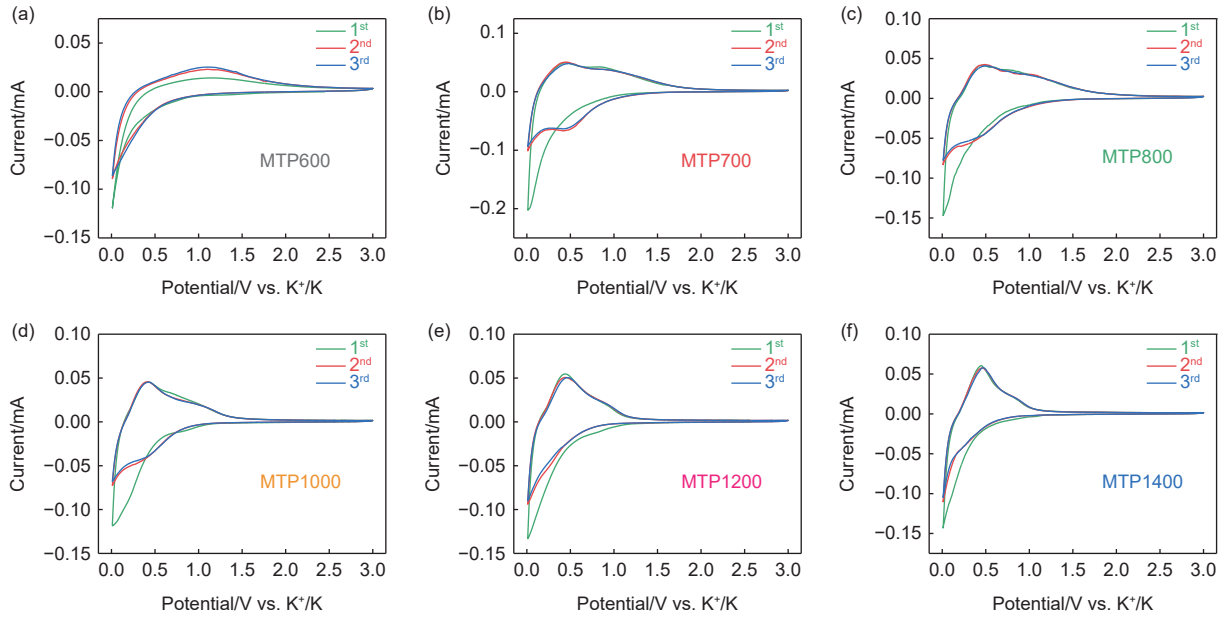

Fig. 4 CV curves at a scan rate of 0.1 mV s^{-1} of MTP samples

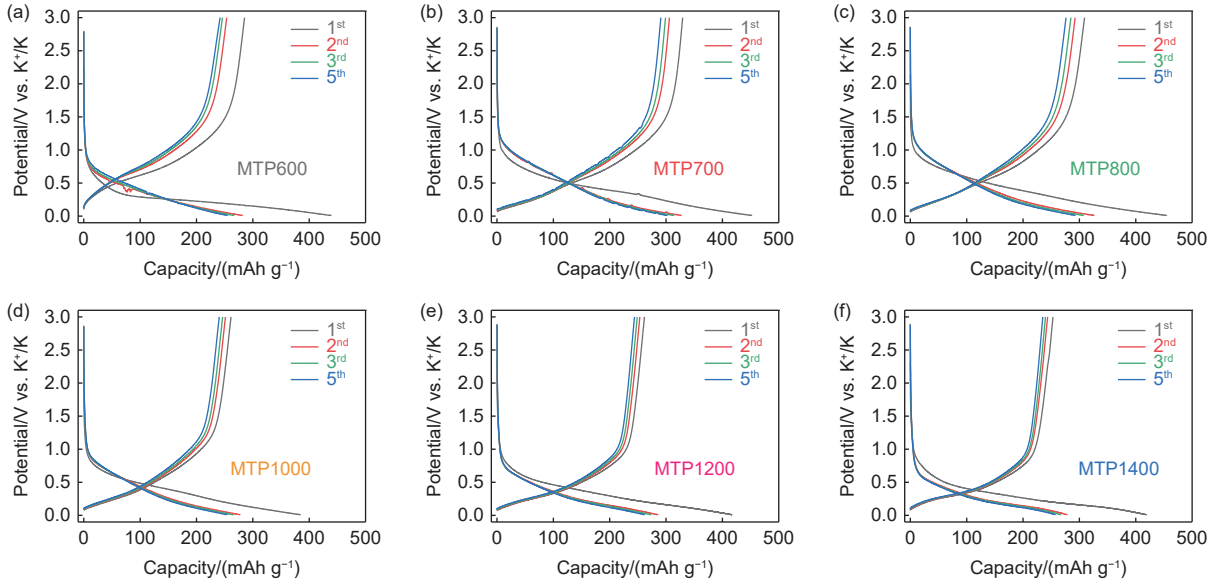

Fig. 5　GCDs at a current density of 0.1 C of MTP samples

changes observed in the CV curves.

The cycle performance of MTP samples was evaluated at a current rate of 0.2 C, as shown in Fig. 6a. There are activation stages in the initial cycles for the carbon material, with K-storage capacity gradually stabilized after 15 cycles. MTP700 exhibits an initial specific capacity of 234.3 mAh g^{-1} and the highest reversible specific capacity of 220.8 mAh g^{-1} after 200 charge-discharge cycles, corresponding to a high capacity retention of 94.2%. As the carbonization temperature rises, the capacity retention initially decreases to 76.0% for MTP800 and 54.0% for MTP1000 and then increases to 78.8% for MTP1200 and 82.1% for MTP1400. Fig. 6b shows the rate performance of MTPs at different current rates. Among them, MTP700, with a higher disordered degree and larger interlayer spacing, exhibits the best rate performance with a reversible specific capacity of 220.0 mAh g^{-1} at a current rate of 0.5 C. A high reversible capacity of 144.2 mAh g^{-1} could be achieved

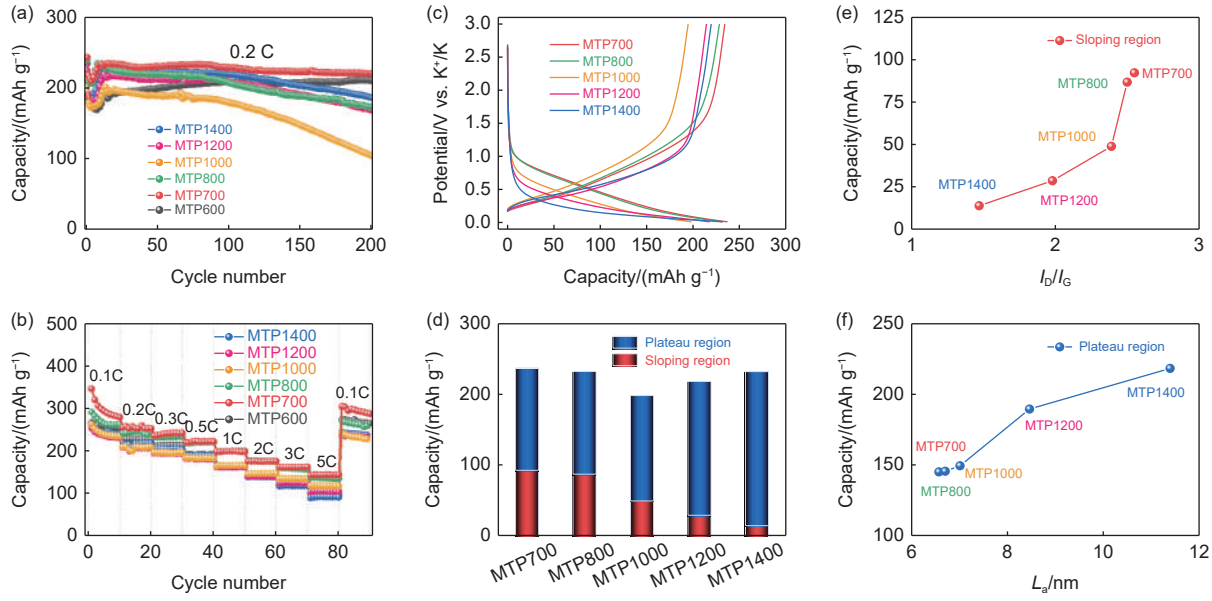

Fig. 6　The comparison of (a) cycle stability at a current density of 0.2 C, (b) rate capability at different current rates, (c) the GCD curves of the 15th cycle, (d) the sloping/plateau region capacity contributions of the discharge processes, and the corresponding relationship with the (e) I_D/I_G values and (f) L_a values of the MTP samples

even at a high current rate of 5 C, indicating its excellent K-storage performance. With the increase of carbonization temperature, the graphitization degree of the carbon materials gradually increases, leading to the enhanced interlayer K-storage behavior. As a result, MTP1000, MTP1200 and MTP1400 exhibit significantly decreased reversible capacities of 118.6, 105.5 and 92.0 mAh g^{-1} at 5 C, respectively, confirming that the higher carbonization temperatures and increased graphitization degrees lead to reduced rate capability for carbon materials.

Furthermore, the stable GCD curves of the 15th cycle at a current rate of 0.2 C were used to investigate the variation of K-storage behaviors of the carbon materials with different carbonization temperatures (Fig. 6c). The typical GCD curves of the carbon materials exhibit a transition from the high-potential sloping region to the low-potential plateau region with increasing the carbonization temperature. Thus, taking 0.5 V as the reference potential, the GCD curves could be divided into the sloping region (>0.5 V) and the plateau region (<0.5 V), with corresponding capacity contributions shown in Fig. 6d. Among all samples, MTP700 delivers the highest capacity in the sloping region (92.3 mAh g^{-1}), while the capacity in the plateau region is only 145.0 mAh g^{-1}. Similarly, MTP800, with a relatively high disordered degree, shows capacity contributions of 86.8 mAh g^{-1} in the sloping region and 145.5 mAh g^{-1} in the plateau region. The sloping region capacity decreases significantly from 48.9 mAh g^{-1} for MTP1000 to 28.6 mAh g^{-1} for MTP1200 while the plateau region capacity increases from 149.3 mAh g^{-1} to 189.6 mAh g^{-1}, respectively. The MTP1400 exhibits the highest plateau region capacity of 218.3 mAh g^{-1} and the lowest sloping region capacity of 13.8 mAh g^{-1}.

These variations are attributed to the structural differences of the carbon materials. Fig. 6e and 6f show the relationship between the sloping region capacity and the I_D/I_G value and the relationship between the plateau region capacity and L_a value, respectively. A high I_D/I_G value corresponding to a higher disordered degree of the carbon materials leads to an increased capacity in the sloping region. On the other hand, the increase in the L_a value of the carbon materials, in relation to improved graphitization degree and microcrystalline size, leads to the improved capacity in the plateau region. Thus, this confirms that the defect content corresponds to the sloping region capacity, while the enhanced microcrystalline size is beneficial for the increase of plateau region capacity during the K-storage process of carbon materials.

The galvanostatic intermittent titration technique (GITT) was used to investigate the kinetic properties of carbon materials under fixed parameters with a pulse current of 0.1 C, a pulse time of 30 min, and a relaxation time of 120 min (Fig. 7a-d). The corresponding K-ion diffusion coefficient (D_{K+}) can be obtained by using the following Equation[37,38]:

$$D_{K+} = \frac{4}{\pi\tau}\left(\frac{m_B V_M}{M_B S}\right)\left(\frac{\Delta E_S}{\Delta E}\right)^2$$

where τ is the pulse time (s), m_B is the mass of active material, M_B is the molar mass of the active material, V_M is the molar volume of the active materials, S is the electrochemically active surface area of the electrode, ΔE_S is the steady-state voltage change, and ΔE_τ is the voltage change during current pulse application. Fig. 7e and 7f shows the variation of calculated D_{K+} during the discharge and charge processes, respectively. A gradual decrease in diffusion coefficient is revealed with the decrease of potential during the discharge process, which should be attributed to the K-storage in the carbon interlayers at the low-potential region. Upon the charge process, there is a noticeable peak below 0.5 V for the diffusion coefficient, and the peak gradually becomes obvious with increasing the carbonization degree, corresponding to the reversible de-intercalation process of K-ion within the interlayers of the carbon materials. Due to its higher disordered degree and larger interlayer spacing, MTP700 exhibits the highest D_{K+}, signifying its excellent K-ion transportation. As the carbonization temperature increases, the graphitization degree of carbon materials gradually increases, leading to an enhanced interlayer K-storage process. However, due to the larger ionic

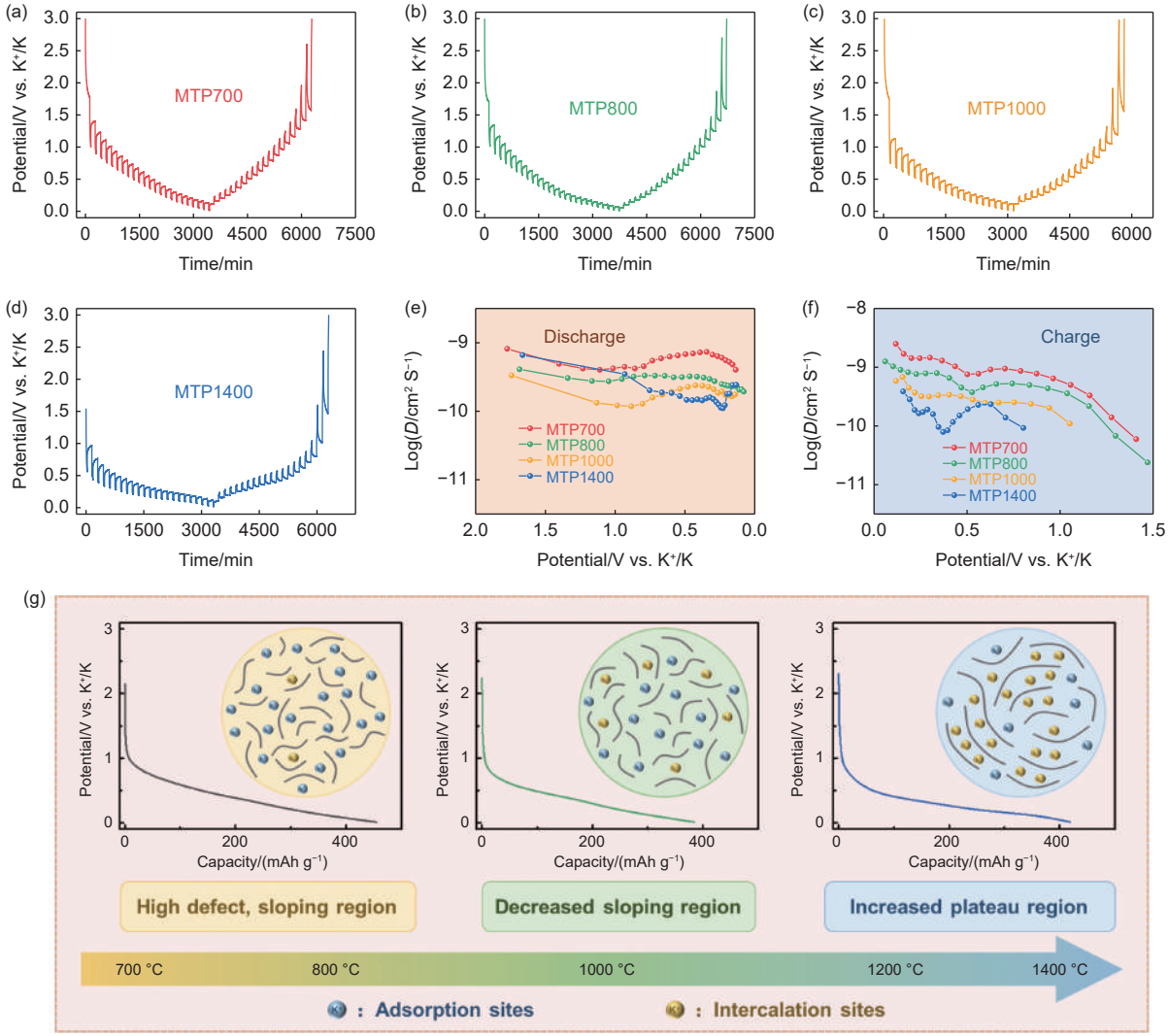

Fig. 7　(a-d) The GITT curves of the 2nd cycle and the corresponding diffusion coefficient at (e) discharge and (f) charge processes of MTP samples. (g) The schematic illustration of the variations of structure and K-storage behavior of pitch-based carbon materials with the carbonization temperature

size of K-ion and smaller interlayer spacing of MTP with the higher graphitization degree, the diffusion coefficient of K-ion between carbon layers is significantly lower than the adsorption K-storage process, resulting in a gradual decrease in D_{K+} value.

Fig. 7g shows a schematic diagram depicting the variation of K-storage behavior with the structural variation of pitch-derived carbon materials produced at different carbonization temperatures. In a low carbonization temperature range (700–1000 °C), the defect content in carbon materials gradually decreases with increasing the carbonization temperature, resulting in a reduction in adsorption potassium storage active sites. Additionally, the microcrystalline size of the carbons remains relatively small, leading to inadequate potassium storage sites between carbon interlayers, and consequently decreased reversible capacity. As the carbonization temperature increases (1000–1400 °C), the graphitization degree of the carbon materials also increases, resulting in a well-developed layered graphite-like carbon structure that provides a large number of interlayer potassium storage active sites, enabling an increase in the plateau region capacity and overall reversible potassium storage capacity of the carbon materials.

4　Conclusion

A series of pitch-based carbon materials were fabricated by adjusting the carbonization temperature. The structures and electrochemical performance of the

derived pitch-based carbon materials were systematically investigated. Among all samples, MTP700 with the optimal disordered degree and larger interlayer spacing exhibits the best K-storage performance that could deliver a high reversible capacity of 329.4 mAh g^{-1}, and a high initial coulombic efficiency of 72.8%. At the same time, the dominated adsorption-typed K-storage behavior enables MTP700 to exhibit a high capacity of 144.2 mAh g^{-1} at a high current rate of 5 C. A comparison of K-storage behaviors and kinetic analysis of the pitch-derived carbons was carried out, and the relationship between carbon structures and K-storage performances was also studied systematically. This work provides a good reference for the future design and development of carbon anode materials for PIBs.

Acknowledgements

This work was financially supported by the National Natural Science Foundation of China (52072021) and the Fundamental Research Funds for the Central Universities (buctrc202141).

References

[1] Dunn B, Kamath H, Tarascon J M. Electrical energy storage for the grid: a battery of choices[J]. Science, 2011, 334(6058): 928-935.

[2] Kubota K, Dahbi M, Hosaka T, et al. Towards K-ion and Na-ion batteries as "beyond Li-ion" [J]. The Chemical Record, 2018, 18(4): 459-479.

[3] Pramudita J C, Sehrawat D, Goonetilleke D, et al. An initial review of the status of electrode materials for potassium-ion batteries[J]. Advanced Energy Materials, 2017, 7(24): 1602911.

[4] Hwang J Y, Myung S T, Sun Y K. Recent progress in rechargeable potassium batteries[J]. Advanced Functional Materials, 2018, 28(43): 1802938.

[5] Jian Z, Luo W, Ji X. Carbon electrodes for K-ion batteries[J]. Journal of the American Chemical Society, 2015, 137(36): 11566-11569.

[6] Luo W, Wan J, Ozdemir B, et al. Potassium ion batteries with graphitic materials[J]. Nano Letters, 2015, 15(11): 7671-7677.

[7] Zhao J, Zou X, Zhu Y, et al. Electrochemical intercalation of potassium into graphite[J]. Advanced Functional Materials, 2016, 26(44): 8103-8110.

[8] Yu J, Jiang M, Zhang W, et al. Advancements and prospects of graphite anode for potassium-ion batteries[J]. Small Methods, 2023, 7(11): 2300708.

[9] Wang D K, Zhang J P, Dong Y, et al. Progress on graphitic carbon materials for potassium- based energy storage[J]. New Carbon Materials, 2021, 36(3): 435-448.

[10] Ran F T, Yang X B, Shao L. Recent progress in carbon-based nanoarchitectures for advanced supercapacitors[J]. Advanced Composites and Hybrid Materials, 2018, 1(1): 32-55.

[11] Adams R A, Varma A, Pol V G. Carbon anodes for nonaqueous alkali metal-ion batteries and their thermal safety aspects[J]. Advanced Energy Materials, 2019, 9(35): 1900550.

[12] Cui R C, Xu B, Dong H J, et al. N/O dual-doped environment-friendly hard carbon as advanced anode for potassium-ion batteries[J]. Advanced Science, 2020, 7(5): 1902547.

[13] Verma R, Singhbabu Y N, Didwal P N, et al. Biowaste orange peel-derived mesoporous carbon as a cost-effective anode material with ultra-stable cyclability for potassium-ion batteries[J]. Batteries & Supercaps, 2020, 3(10): 1099-1111.

[14] Alvin S, Chandra C, Kim J. Controlling intercalation sites of hard carbon for enhancing Na and K storage performance[J]. Chemical Engineering Journal, 2021, 411: 128490.

[15] Zhu T, Mai B, Hu P, et al. Bagasse-derived hard carbon anode with an adsorption –intercalation mechanism for high-rate potassium storage[J]. ACS Applied Energy Materials, 2023, 6(4): 2370-2377.

[16] Tao L, Liu L, Chang R, et al. Structural and interface design of hierarchical porous carbon derived from soybeans as anode materials for potassium-ion batteries[J]. Journal of Power Sources, 2020, 463: 228172.

[17] Wang B, Yuan F, Wang J, et al. Multi-forks hierarchical porous amorphous carbon with N-Doping for high-performance potassium-ion batteries[J]. Electrochimica Acta, 2020, 354: 136627.

[18] Yin J, Jin J, Chen C, et al. Preferential pyrolysis construction of carbon anodes with 8400 h lifespan for high-energy-density K-ion batteries[J]. Angewandte Chemie International Edition, 2023, 62(17): e202301396.

[19] Zhu F, Cao W, Song W, et al. Biomass-derived carbon prepared through a quadruple-functional-salt approach for application in K-ion capacitors[J]. Chemical Engineering Journal, 2022, 449: 137561.

[20] Yuan F, Zhang D, Li Z, et al. Unraveling the intercorrelation between micro/mesopores and K migration behavior in hard carbon[J]. Small, 2022, 18(12): 2107113.

[21] Tan H, Zhou R, Zhang B. Understanding potassium ion storage mechanism in pitch-derived soft carbon and the consequence on cyclic stability[J]. Journal of Power Sources, 2021, 506: 230179.

[22] Liu Y, Lu Y X, Xu Y S, et al. Pitch-derived soft carbon as stable anode material for potassium ion batteries[J]. Advanced Materials, 2020, 32(17): 2000505.

[23] Liu H, Du H, Zhao W, et al. Fast potassium migration in mesoporous carbon with ultrathin framework boosting superior rate performance for high-power potassium storage[J]. Energy Storage Materials, 2021, 40: 490-498.

[24] Wu S, Song Y, Lu C, et al. High-rate soft carbon anode in potassium ion batteries: The role of chemical structures of

pitches[J]. Carbon, 2023, 203: 211-220.

[25] Wu S, Song Y, Lu C, et al. An adsorption-insertion mechanism of potassium in soft carbon[J]. Small, 2021, 18(4): 2105275.

[26] Jiang M, Sun N, Ali Soomro R, et al. The recent progress of pitch-based carbon anodes in sodium-ion batteries[J]. Journal of Energy Chemistry, 2021, 55: 34-47.

[27] Ma X, Xiao N, Xiao J, et al. Nitrogen and phosphorus dual-doped porous carbons for high-rate potassium ion batteries[J]. Carbon, 2021, 179: 33-41.

[28] Sun N, Qiu J S, Xu B. Understanding of sodium storage mechanism in hard carbons: Ongoing development under debate[J]. Advanced Energy Materials, 2022, 12(27): 2200715.

[29] Zhao R, Sun N, Xu B. Recent advances in heterostructured carbon materials as anodes for sodium-ion batteries[J]. Small Structures, 2021, 2(12): 2100132.

[30] Chang X Q, Sun N, Zhou H Y, et al. Soft carbon-coated bulk graphite for improved potassium ion storage[J]. Chinese Chemical Letters, 2023, 34(3): 107312.

[31] Jiang M, Sun N, Li T, et al. Revealing the charge storage mechanism in porous carbon to achieve efficient K ion storage[J]. Small, 2024: 2401478.

[32] Hou Z, Jiang M, Lei D, et al. Regulation of pseudographitic carbon domain to boost sodium energy storage[J]. Nano Research, 2024, 17(6): 5188-5196.

[33] Zhang X, Hou Z, Jiang M, et al. Molecular engineering to regulate the pseudo-graphitic structure of hard carbon for superior sodium energy storage[J]. Small, 2024: 2311778.

[34] Alvin S, Cahyadi H S, Hwang J, et al. Revealing the intercalation mechanisms of lithium, sodium, and potassium in hard carbon[J]. Advanced Energy Materials, 2020, 10(20): 2000283.

[35] Cançado L G, Takai K, Enoki T, et al. General equation for the determination of the crystallite size La of nanographite by Raman spectroscopy[J]. Applied Physics Letters, 2006, 88(16): 163106.

[36] Sadezky A, Muckenhuber H, Grothe H, et al. Raman microspectroscopy of soot and related carbonaceous materials: Spectral analysis and structural information[J]. Carbon, 2005, 43(8): 1731-1742.

[37] Zhang S, Sun N, Li X, et al. Closed pore engineering of activated carbon enabled by waste mask for superior sodium storage[J]. Energy Storage Materials, 2024, 66: 103183.

[38] Chen H, Sun N, Wang Y, et al. One stone two birds: Pitch assisted microcrystalline regulation and defect engineering in coal-based carbon anodes for sodium-ion batteries[J]. Energy Storage Materials, 2023, 56: 532-541.